http://www.press.ierek.com

ISSN (Print: 2357-0849, online: 2357-0857)

Environmental Science and Sustainable Development

Research Paper

Received: 08 January 2025, Accepted: 27 April 2025, Published online: 30 June 2025

**DOI: 10.21625/essd. v10i2.1168**

# Performance of Biogenic Silica Photocatalytic Ceramic Foams and Cu-$TiO_2$ NPs in the Degradation of Emerging Pollutants under Natural Solar Radiation

**Yhosmary Franco[1], Jimmy Castillo[2], Juan C. Pereira[3]**

*[1]PhD Candidate, Technological Chemistry, Experimental Faculty of Sciences and Technology, University of Carabobo, Valencia, Venezuela*

*[2] Full Professor, School of Chemistry, Faculty of Sciences, Central University of Venezuela, Caracas, Venezuela*

*[3] Full Professor, Department of Chemistry, Experimental Faculty of Sciences and Technology, University of Carabobo, Venezuela*

## Abstract

Emerging contaminants in the drinking water supply are a growing concern due to their presence in various sources and incomplete degradation occurring in conventional treatment plants. This underscores the need to implement alternative and specialized processes for their removal. Photocatalysis, an advanced oxidation process that uses radiation as the sole energy source, is emerging as a promising solution. In this study, the performance of novel photocatalytic materials was evaluated: ceramic foams synthesized from biomass, specifically biogenic silica obtained from rice husk, and copper-decorated titanium dioxide nanoparticles (Cu-$TiO_2$ NPs). These foams were synthesized using the direct foaming method with $CO_2$, an efficient and sustainable approach. Their performance was evaluated in the degradation of acetaminophen (ACP), an emerging contaminant of pharmaceutical origin, achieving a removal of 91.0% with a loading of 1.5 g/L, a time of 83 minutes and using natural solar radiation. The results obtained demonstrate that these ceramic foams have the potential to overcome current limitations and represent a significant advance towards the implementation of photocatalysis on an industrial and global scale.

© 2025 The Authors. Published by IEREK Press. This is an open-access article under the CC BY license (https://creativecommons.org/licenses/by/4.0/). Peer review under the responsibility of ESSD's International Scientific Committee of Reviewers.

***Keywords***

*Photocatalysis; Ceramic foam; Biogenic silica; Titanium dioxide; Emerging contaminants.*

## 1. Introduction

Pharmaceuticals and personal care products (PPCPs) are emerging contaminants present in water resources. ACP is an example of such contaminants and is found in prescription medications. Globally, about 1.4×105 tons/year of ACPs are consumed, indicating their potential impact on the environment (Gupta *et al*., 2023). Pharmaceutical contaminants can cause adverse health effects, such as aquatic toxicity and the development of resistance in pathogens. These compounds reach water bodies through various sources, such as direct disposal of surplus drugs, excretion by humans and animals, and inadequate treatment of manufacturing effluents (Yang *et al*., 2008).

Emerging contaminants are persistent due to their resistance to conventional wastewater treatments and are increasingly present in the environment. To significantly reduce the presence of pharmaceutical compounds in

discharged effluents, additional treatments need to be implemented. Advanced oxidation processes (AOP) have proven to be effective for this purpose. AOP can be carried out as a tertiary treatment following biological (secondary) treatment, or as a pretreatment stage to improve the biodegradability of trace organic contaminants (Gonzalez *et al*., 2016).

Heterogeneous photocatalysis, an AOP, is based on the excitation of a solid, usually a wide energy gap semiconductor such as $TiO_2$, by irradiation whose energy is equal to or greater than its energy gap. This excitation causes the transition of an electron from the valence band (VB) to the conduction band (CB), generating photogenerated electron-hole pairs ($e^-/h^+$) (Reaction 1). The holes (h+) can react with water molecules ($H_2O$) or hydroxyl groups (-OH) adsorbed on the surface, producing hydroxyl radicals (HO•) (Reactions 2 and 3), which have a high oxidative potential (approx. 1.7 mV) and are highly reactive with organic matter, resulting toxic to microorganisms (Reactions 10) (Fujishima & Honda, 1972). Furthermore, oxygen present in the air can function as a receptor for photogenerated electrons (e-) by reacting with them to form superoxide radical anions ($\bullet O_{2^-}$), which in turn react with water to produce hydroxyl radicals (Reactions 4 and 5). These reactions trigger a series of processes that contribute to the photocatalytic degradation of organic pollutants (Reactions 6 – 9) (Espiga, 2018).

$$TiO_2 + h\nu \rightarrow TiO_2\ (e^-_{cb} + h^+_{vb})\ (1)$$

$$h^+_{vb} + H_2O \rightarrow H^+ + \bullet OH\ (2)$$

$$h^+_{vb} + {}^-OH \rightarrow \bullet OH\ (3)$$

$$e^-_{cb} + O_2 \rightarrow \bullet O_2^-\ (4)$$

$$\bullet O_2^- + H_2O \rightarrow HO_2\bullet + \bullet OH\ (5)$$

$$HO_2\bullet + H_2O \rightarrow H_2O_2 + \bullet OH\ (6)$$

$$e^-_{cb} + H_2O_2 \rightarrow \bullet OH + HO^-\ (7)$$

$$H_2O_2 + h\nu \rightarrow 2HO\bullet\ (8)$$

$$H_2O_2 + \bullet O_2^- \rightarrow \bullet OH + HO^- + O_2\ (9)$$

$$R\ /\ microorganism + \bullet OH \rightarrow Degradation\ products\ (10)$$

$TiO_2$ has characteristics such as being non-toxic, corrosion-resistant, biocompatible, low-cost, and with a high density of active sites (Nevárez *et al*., 2017). Despite its advantages, the use of $TiO_2$ as a photocatalyst has faced limitations due to its wide energy gap, which restricts its activation capacity under visible radiation. However, interest in using sunlight to activate photocatalysts has been increasing, due to its multiple advantages, such as its abundance, natural availability, and low cost (Rodríguez & Barrera, 2020). In this sense, research has been conducted to reduce the energy gap of $TiO_2$, to take full advantage of 43% of the solar irradiation spectrum. Among the main modifications are the implantation of metal ions, doping with metals and non-metals, among others. It has been observed that doping of $TiO_2$ with copper tends to increase the photocatalytic activity of the material under visible radiation, reducing the recombination of charge carriers (Kaur *et al*., 2021).

Photocatalysis has proven effective in removing organic micropollutants at the laboratory level, but its industrial application has been limited. Photocatalysts in the form of NPs dispersed in water or sludge have the drawback of requiring expensive removal processes to avoid leaching into water streams. On the other hand, immobilized catalysts have been developed to address this problem, although they have a smaller photocatalytic active surface area, which affects their efficiency. However, photocatalytic foams have the potential to overcome these limitations and move towards the industrial scalability of photocatalysis (Warren *et al*., 2023). Photocatalytic ceramic foams offer enormous potential in terms of efficiency, effectiveness, and most importantly, scalability. Materials with two different levels of porosity, microporous and macroporous, can efficiently convert irradiation into oxidative species that promote the degradation of micropollutants (Ochuma *et al*., 2007).

The purpose of this research was to analyze the performance of photocatalytic ceramic foams, synthesized from biogenic silica obtained from rice husks and pure $TiO_2$ NPs, as well as Cu-$TiO_2$ NPs, in the degradation of ACP using natural solar radiation.

## 2. Materials and methods

The research design used in this study corresponds to an experimental approach, in which experiments are conducted with rigorous control of the variables. These include concentration, pH, photocatalyst loading and reaction conditions. This approach allows the effect of independent variables on dependent variables to be analyzed, using random assignment of treatments to ensure the validity of the results.

### 2.1. Chemicals

Commercial reagent-grade products were used without the need for added purification. Among the products used were $TiO_2$ anatase 99.5% from Sensient, sodium chloride (NaCl) 100.1% (MW= 58.44 g/mol) from Fisher Chemical, sodium hydroxide (NaOH) 96% (MW= 40.0 g/L) from Erba, copper (II) sulfate pentahydrate ($CuSO_4 \cdot 5H_2O$) 99% (MW= 249.68 g/mol) from EMSURE, rice husks from Venezuelan crops (RH), phosphoric acid ($H_3PO_4$) 85% (MW= 97.994 g/mol) from Fisher Chemical, potassium hydroxide (KOH) 85% (MW= 56.11 g/mol) from Fisher Chemical, carbon dioxide ($CO_2$), monosodium phosphate ($NaH_2PO_4 \cdot H_2O$) 99% (MW= 137.99 g/mol) from Fisher Chemical, and paracetamol ($C_8H_9NO_2$) Lote: BP-03/11/08 from G. Amphray Laboratories.

### 2.2. Synthesis of ceramic foams

To synthesize ceramic foams, the following steps were followed: first, $TiO_2$ NPs were obtained by mechanical grinding of commercial $TiO_2$ with NaCl as an inorganic dispersant, using a Leegol Electric PG-LG-002 ball mill. Then, the wet impregnation method was used with 1% by weight of $CuSO_4 \cdot 5H_2O$ as a doping precursor, dissolving the $CuSO_4 \cdot 5H_2O$ in distilled water and mixing it with the $TiO_2$ NPs. The mixture was stirred at 50 °C for 2 hours (Faithful SH-2 hot plate), and the pH was adjusted to 8 with 1 M NaOH. Subsequently, it was dried at 90 °C for 24 hours, calcined at 450 °C for 2 hours and finally washed and dried again at 90 °C in a Raypa oven.

Biogenic silica was obtained from rice husk ash (RHA) following the protocol of Castillo *et al*. (2022). This silica was dissolved in KOH and mixed with the $TiO_2$ NPs, subjecting it to ultrasound for 15 minutes with an Elmasonic E30H equipment. The mixture was bubbled with $CO_2$ and dried at 80 °C for 24 hours. In this way, two types of ceramic foam were produced: EC0 (with $TiO_2$ NPs) and EC1 (with Cu-$TiO_2$ NPs).

### 2.3. Characterization

In the present study, tests were conducted to characterize the properties of the synthesized $TiO_2$ NPs, as well as those of the ceramic foams. For this purpose, the X-ray diffraction (XRD) technique was used to determine both the crystalline structure and the size of the $TiO_2$ crystals. The analysis was performed using a D2 PHASER XRD Bruker equipment, belonging to the Institute of Advanced Studies Foundation (IDEA). This equipment operated at 30 kV and 10 mA, using Cu Kα radiation. The sensor was scanned in a 2θ angle range of 10° to 70°, with a step size of 0.02° and a time per step of 1 second. In addition, a wavelength of 1.541840 Å and an incidence window of 0.2 mm were used. These experimental conditions allowed precise data to be obtained for the structural and morphological characterization of the analyzed samples.

From the broadening of the peak corresponding to the anatase phase (101), the average size of the crystals of both the $TiO_2$ and Cu-$TiO_2$ NPs was estimated, applying the Scherrer equation (Equation 1) (Moongraksathum *et al*., 2018):

$$L = \frac{0{,}9\lambda}{\beta cos\theta} \quad (1)$$

In the formula given, L is the average crystallite size, λ is the X-ray wavelength (0.154184 nm), β refers to the full width at half maximum (FWHM) in radians, and θ is the diffraction angle.

On the other hand, the ceramic foams were analyzed by XRD using a LANScientific Fringe Class 65410034 equipment, belonging to the School of Geology and Mines of the Faculty of Engineering of the Central University of Venezuela (UCV). This analysis was conducted under a configuration of 30 kV and 16 mA, using Cu Kα radiation with a wavelength of 1.54060 Å. Additionally, morphological characterization and elemental analysis were conducted by scanning electron microscopy (SEM) and X-ray dispersive spectroscopy (EDS). For this, a JEOL JSM-6390

equipment was used, equipped with an Oxford Instruments model 7582 X-ray detector, belonging to the Simón Bolívar University (USB).

## 2.4. Evaluation of photocatalytic activity

The photocatalysis experiments were conducted under natural solar radiation during sunny days in the months of August, September, and October of the year 2024. The initial total radiation recorded was 924 W/m², measured with a digital radiometer. These tests were conducted at the School of Chemistry of the Faculty of Sciences of the UCV, located at the geographic coordinates 10.487348333689186, -66.8958709428127. The experimental system (Figure 1) consisted of a cylindrical borosilicate reactor operated in batch mode, with a volume of 200 mL of ACP solution and a ceramic foam loading of 1.5 g/L. The reactor operated under constant magnetic stirring and with continuous oxygen injection from a continuous air flow of $8.33\times10^{-6}$ m³/s, equivalent to 105 mL/min of oxygen, using a Penn-Plax Airtech 2K0 aquarium air pump. Samples were taken at specific time intervals: 17, 33, 50, and 83 minutes. Control tests were also performed, including photolysis (without photocatalytic material) and adsorption under dark conditions.

For in situ monitoring, the Raman Spectroscopy technique was used using the Eddu Raman TO-ERS-532 system, manufactured by Thunder Optics and belonging to the Nanotechnology and Spectroscopy Laboratory of the UCV. This equipment is equipped with an AvaSpec-Mini spectrometer from the Avantes brand, which incorporates a 2048-pixel CMOS detector and a spectral resolution of 0.09 nm. In addition, the system includes a 532 nm laser with a line width of 0.1 nm, an optical fiber, and a compact Raman probe with a range for Raman shifts up to 175 $cm^{-1}$. It also has a 20X NA 40 microscope objective with a working distance of 11.8 mm, a fixed slit of 50 µm and AvaSoft 8 software for data acquisition and management. The laser operated with a power of 2.8 mW and a spectral acquisition time of 2 seconds. The data obtained were processed and visualized using SpectraGryph software version 1.2.

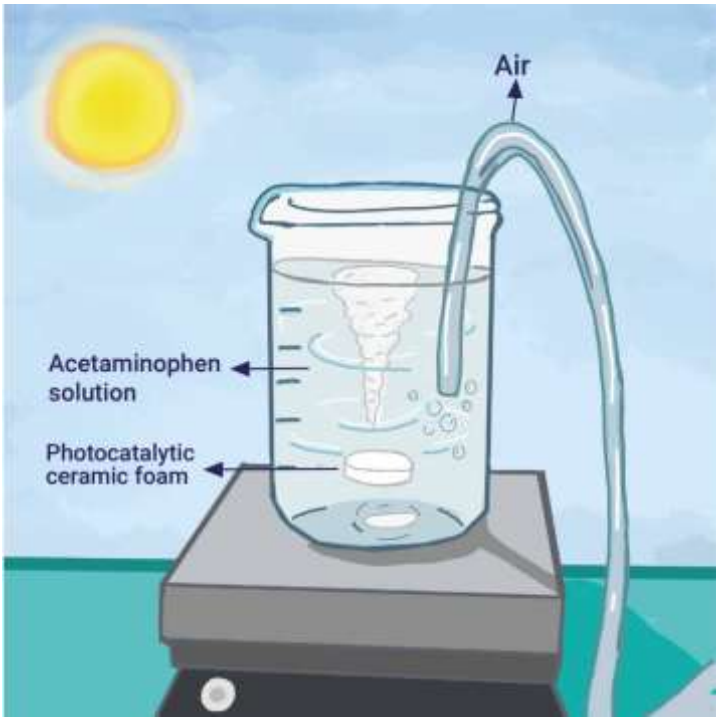


Figure 1: Photocatalytic reaction system with natural solar radiation. (Source: Drawing by Sandra Triana)

## 3. Results and discussion

## 3.1. Characterization of ceramic foams

The crystalline structure of the nanophotocatalysts ($TiO_2$ NPs and Cu-$TiO_2$ NPs) prepared in this investigation was evaluated by the XRD technique. Figure 2 depicts the XRD patterns of the undecorated and 1% Cu-decorated $TiO_2$ NPs samples, which show several well-defined diffraction peaks. The peaks observed at 2θ = 25.10°, 36.56°, 37.40°,

38.16°, 47.48°, 53.22°, 54.38°, 61.90° and 67.88° correspond to the anatase $TiO_2$ crystal plains (101), (103), (004), (112), (200), (105), (211), (204) and (116), respectively, coinciding with card number 00-900-8216.

The XRD patterns show no evidence of the presence of copper oxides, suggesting that the Cu atoms are in a uniformly dispersed state. In addition to the characteristic $TiO_2$ peaks, the absence of impurity peaks demonstrates that no aggregated phases are generated during the Cu-$TiO_2$ NPs synthesis method used in this investigation. Despite using different synthesis methods, these results are consistent with previous research by Dorraj *et al*. (2017), J. C. Lin *et al*. (2018), Preda *et al*. (2022) and Raheem *et al*. (2023).

Calculations performed from Equation 1 indicate that the crystallite sizes are 21.44 nm for $TiO_2$ NPs and 20.36 nm for Cu-$TiO_2$ NPs. The radiation decrease in particle size might be the result of the interaction between copper and $TiO_2$. These results are consistent with previous studies reported by Turkten *et al*. (2019), Manga *et al*. (2019), Preda *et al*. (2022) y Leong *et al*. (2022).

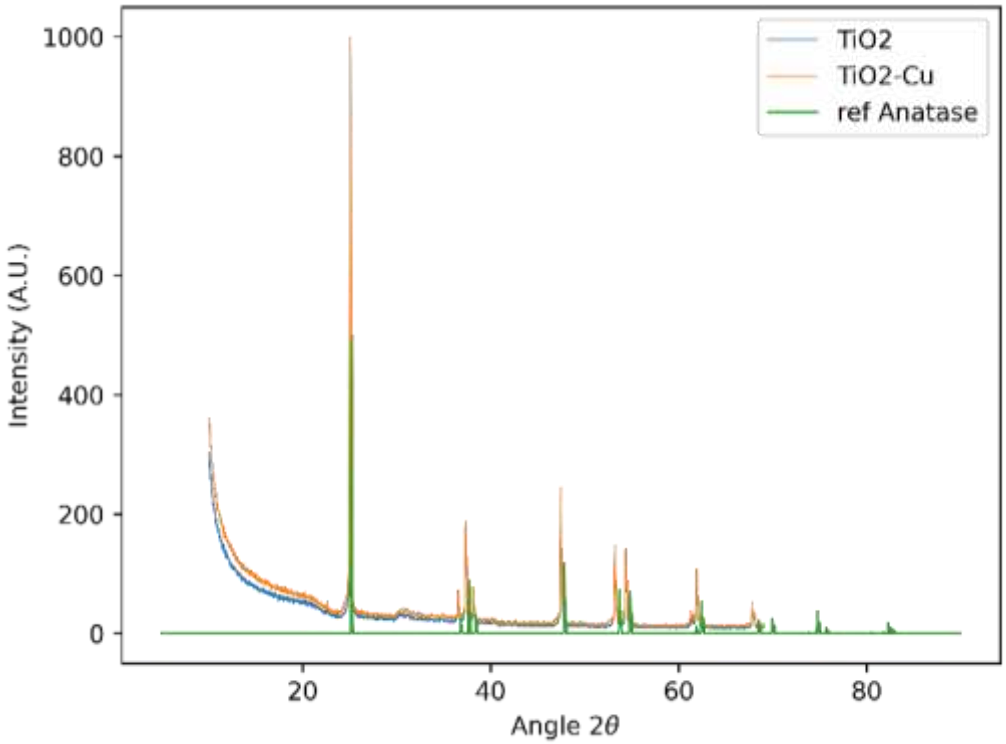


Figure 2: XRD patterns of $TiO_2$ NPs samples (blue), Cu-$TiO_2$ NPs (orange) and anatase reference (green). (Source: made by the authors)

The results are significant since $TiO_2$ NPs function as photocatalysts in the ceramic foams developed in this study. These NPs have been found to be in their anatase phase, which is considered the most active in radiation-accelerated catalysis processes (Aguilar *et al*., 2022). Likewise, the nano-scale particle size of the photocatalytic materials has a crucial impact on the optical behavior of the mixture, as well as on the distribution of radiation within the reactor and the efficiency of the photocatalytic process (Cassano & Alfano, 2000).

An analysis using the XRD technique was performed to determine the structure of the synthesized ceramic foams. The X-ray diffractogram of the EC0 ceramic foams is presented in Figure 3. The XRD results showed a broad peak centered at 2θ between 20° and 30°, without the presence of sharp peaks, showing the amorphous nature of the biogenic silica obtained from rice husk ash. No crystalline silica phases were seen in the XRD patterns, suggesting that the $SiO_2$ in the ash is amorphous. In addition, diffraction peaks related to the anatase crystalline phase of $TiO_2$ were found, as mentioned above. These results are consistent with previous studies conducted by Fernández *et al*. (2019), Porrang *et al*. (2021), Hoerudin *et al*. (2022), Shrestha *et al*. (2023) y Pereira *et al*. (2023).

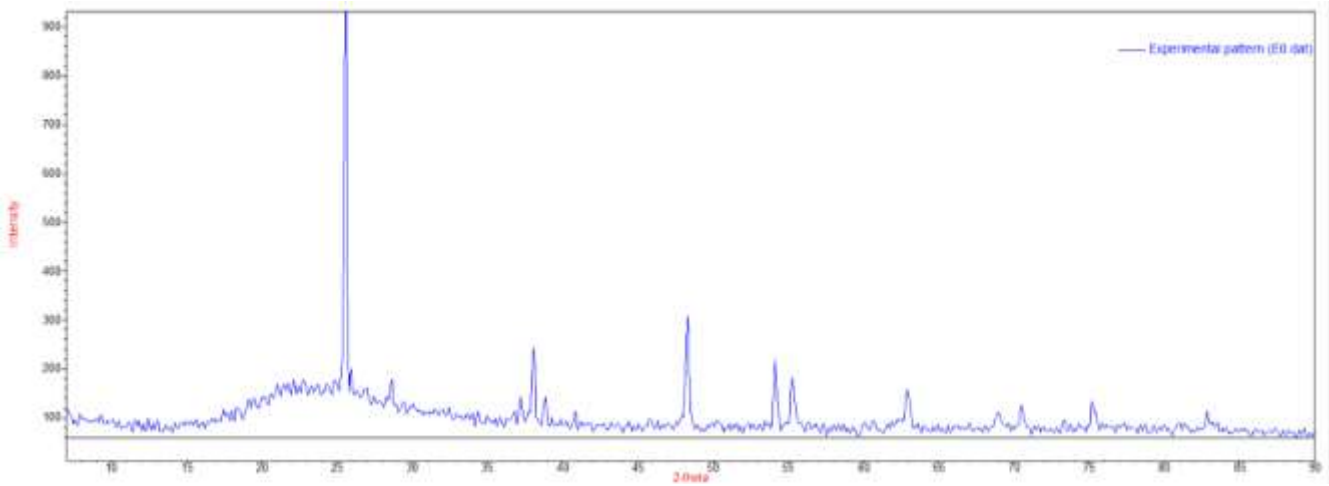

Figure 3: XRD pattern of the photocatalytic ceramic foam EC0. (Source: made by the authors)

The photocatalytic ceramic foam EC0 was characterized using the SEM technique, the results of which are presented in Figure 4. A rough morphology was observed, composed of a structure of agglomerates of hemispherical particles with an average size of 0.22 µm. The image reveals that the surfaces have dark pigmentation, which corresponds to porous cavities. These pores have an irregular shape and a size that varies between 0.1 µm and 0.4 µm.

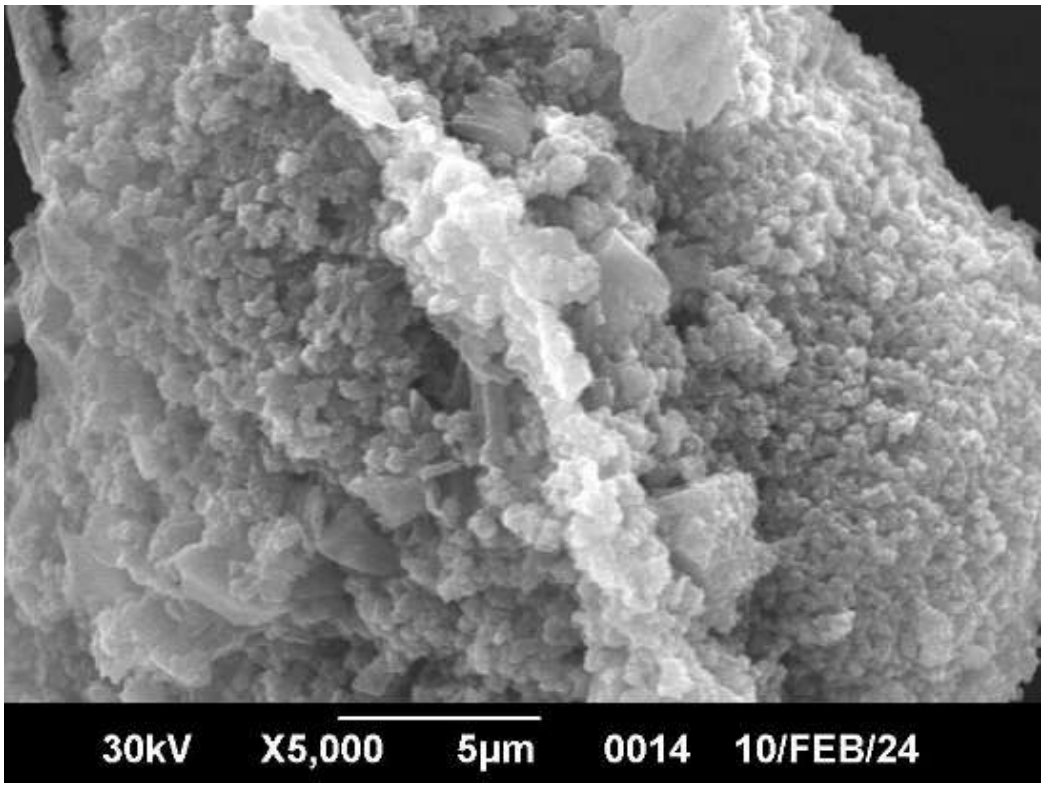


Figure 4: SEM micrograph of the EC0 photocatalytic ceramic foam. (Source: made by the authors)

To better understand the interaction between the biogenic silica matrix and the $TiO_2$ NPs, a SEM-EDS analysis was conducted. When seeing the EDS spectrum of samples EC0 (Figure 5a) and EC1 (Figure 5b), a composition rich in Si and Ti atoms is evident. In both spectra, the high oxygen content (57% and 48%, respectively) is consistent with the presence of the $SiO_2$ and $TiO_2$ network. In addition, the presence of K atoms, originating from the solvent used in the synthesis, is seen, and in the case of the EC1 foam made up of $SiO_2$/Cu-$TiO_2$ NPs, the presence of copper was detected, as expected (See Table 1).

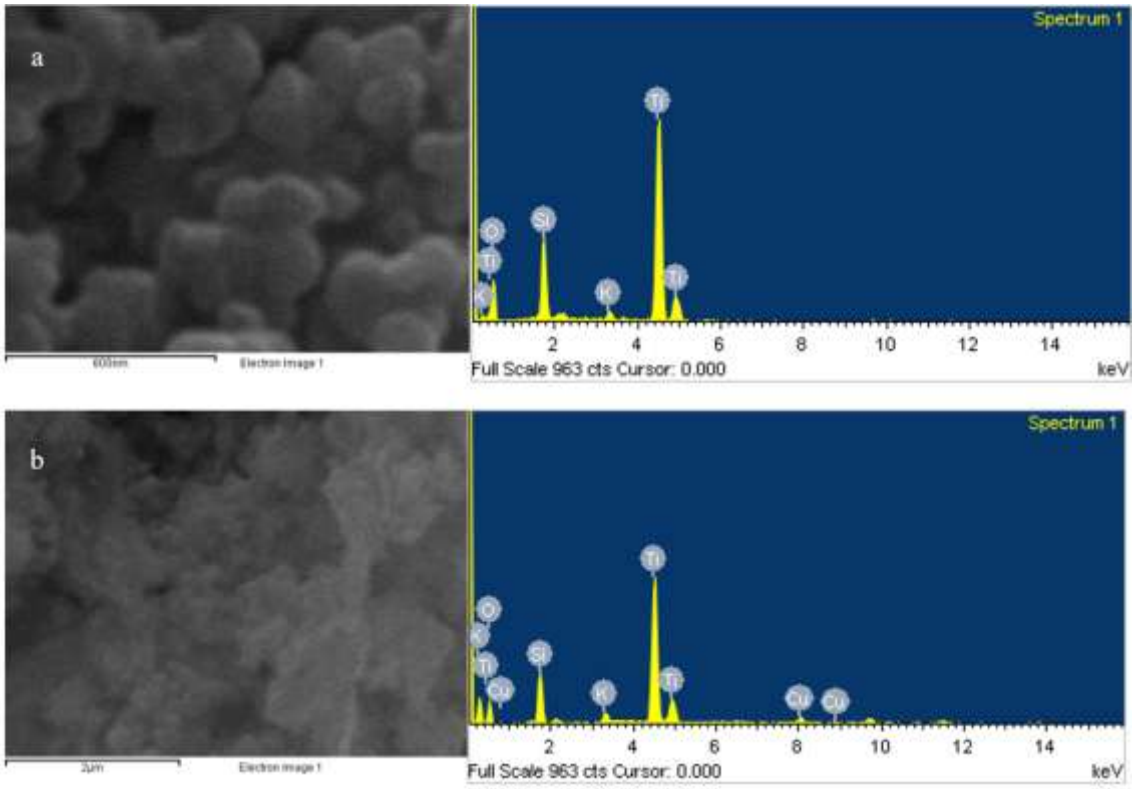


Figure 5: SEM-EDS analysis of EC0 (a) and EC1 (b). (Source: made by the authors)

Table 1: EDS analysis of photocatalytic ceramic foams.

| Sample | Element | %Weight | %Atomic |
|---|---|---|---|
| **EC0** | O | 57.78 | 77.13 |
| | Si | 9.89 | 7.65 |
| | K | 0.91 | 0.50 |
| | Ti | 32.42 | 14.71 |
| **EC1** | O | 48.19 | 68.45 |
| | Si | 20.2 | 16.68 |
| | K | 2.21 | 1.29 |
| | Ti | 27.54 | 13.06 |
| | Cu | 1.44 | 0.52 |

## 3.2. Photocatalytic activity

During the in situ monitoring of the photocatalytic reaction, the Raman spectroscopy technique was employed, which has been widely used in drug quantification studies (Borio *et al*., 2012). Raman spectroscopy is a technique that allows the measurement of the vibration modes of a sample, which provides detailed information about its chemical composition. The resulting spectrum shows a distribution of peaks corresponding to the specific molecular vibrations

of the analyzed sample. These peaks can be used to identify and quantify chemical substances, such as drugs, based on their frequency and intensity (Shende *et al*., 2014).

In pharmaceutical manufacturing and finished product testing, figuring out drug content through high-performance liquid chromatography (HPLC) testing is a time-consuming and potentially destructive process. In contrast, Raman spectroscopy has appeared as a widely used technique for the quantification of active pharmaceutical ingredients (APIs) and excipients in drugs, as well as for the identification and quantification of crystal polymorphism. This technique is rapid, convenient, noninvasive, and nondestructive, allowing for the minimization of sample preparation and providing highly specific information on the chemical composition of dense and highly turbid samples. Furthermore, being a solvent-free technique, Raman spectroscopy is positioned as an attractive and promising tool in the framework of green chemistry (De Bleye *et al*., 2013; Mojica *et al*., 2018; Zhao *et al*., 2022).

ACP is composed of an aromatic ring, a carbonyl group (C=O), an alcohol group and nitrogen (Figure 6). In the specific case of ACP, its Raman spectrum (Figure 7a) is dominated by characteristic peaks such as the amide I (C=O) at 1625 $cm^{-1}$, the amide II (C-N stretching, N-H bending) at 1575 $cm^{-1}$, the C–H bond at 1225 $cm^{-1}$, and the phenyl ring at 800 $cm^{-1}$. The peaks at 1175 $cm^{-1}$, 1275 $cm^{-1}$, and 1325 $cm^{-1}$ were separately derived from the C-N-C symmetric stretching vibration, the benzene –OH stretching vibration, and the $CH_3$ symmetric variant, respectively. Two of these peaks (1225 and 1625 $cm^{-1}$) are only observed for ACP and can be used as marker peaks to identify and quantify any sample containing ACP (Mojica *et al*., 2018; Zhao *et al*., 2022).

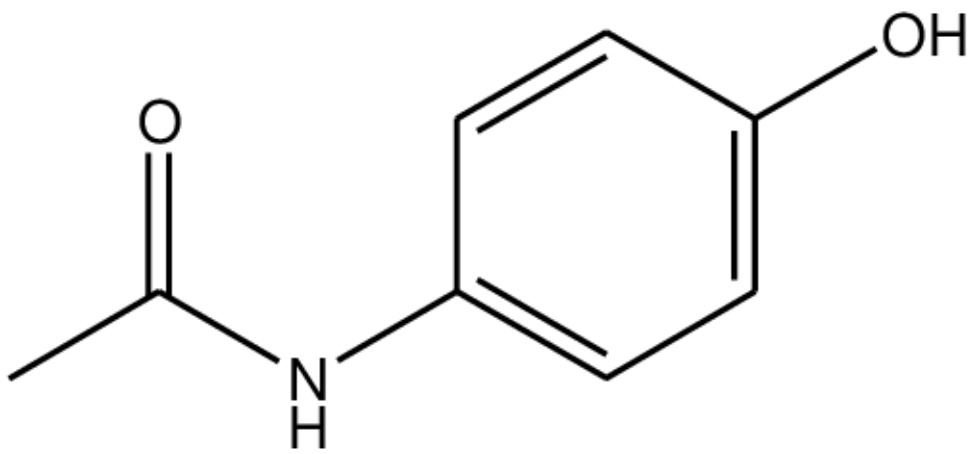


Figure 6: Chemical structure of ACP. (Source: Srabovic *et al*. ,2017)

In this research, the conventional method of measuring Raman peak intensities (area) was used to quantify ACP. The peak at 1600 was chosen to conduct the quantitative analysis of ACP, which corresponds to C=O stretching with the contribution of ring stretching (C=C) (Figure 7b). A calibration curve was performed with ACP solutions in a concentration range from 2 ppm to 14 ppm (Figure 7c), starting from the principle that the amount of active ingredient has a direct effect on the generated signal. The most reported validation criteria are the coefficient of determination ($R^2$) of the calibration curve, which in this study was 0.9849, and the concentration range, to evaluate the relationship between concentration and Raman signal in quantitative detections. In the linear calibration range, the concentration is estimated by linear regression (Cailletaud *et al*., 2018).

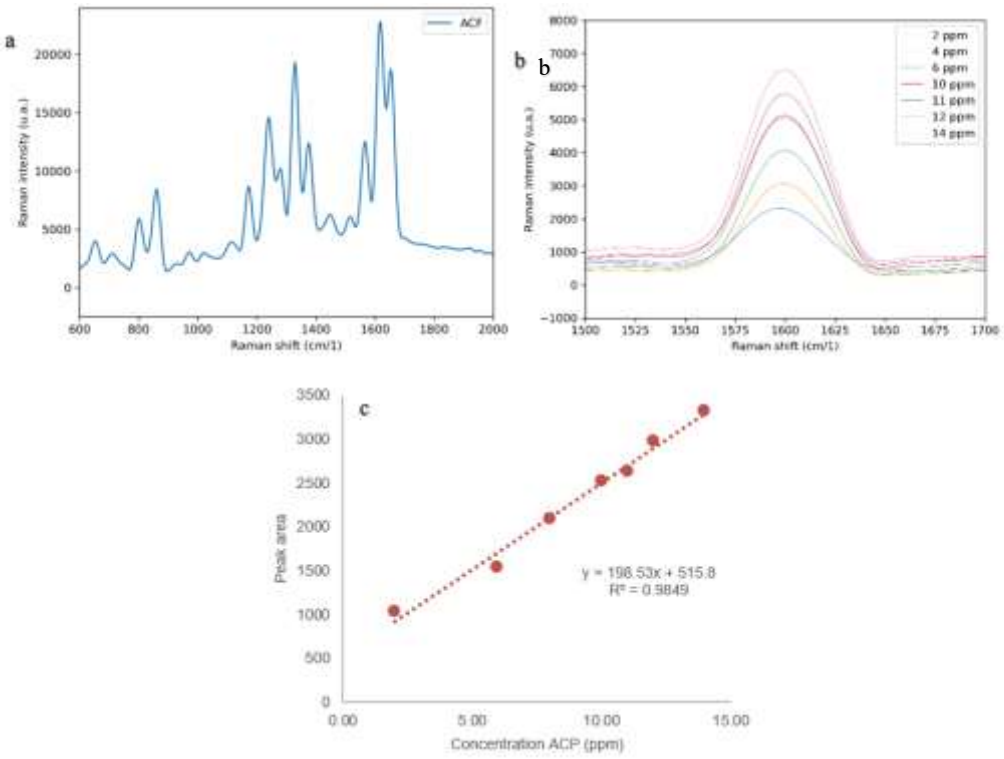


Figure 7: Raman spectrum of ACP (a), zoom to Raman peak at 1600 $cm^{-1}$ at different ACP concentrations (b) and calibration curve of ACP (c). (Source: made by the authors)

By applying this method, the ACP solutions treated photocatalytically with EC0 and EC1 were analyzed under natural solar irradiation, using Raman spectroscopy as a characterization technique. Figure 8 presents the graph illustrating the ACP degradation efficiency as a function of time. Initially, an adsorption process was identified in the foams that reached an average of 29%, which represents a key stage within the photocatalytic mechanism (Ugarteburi, 2018).

Regarding the efficiency of photocatalytic degradation, the results indicate that the use of 1.5 g/L of the EC1 allowed a 91.0% degradation of the ACP to be achieved in a period of 83 minutes. In comparison, under the same load and time conditions, the maximum efficiency obtained with EC0 was 68.3%.

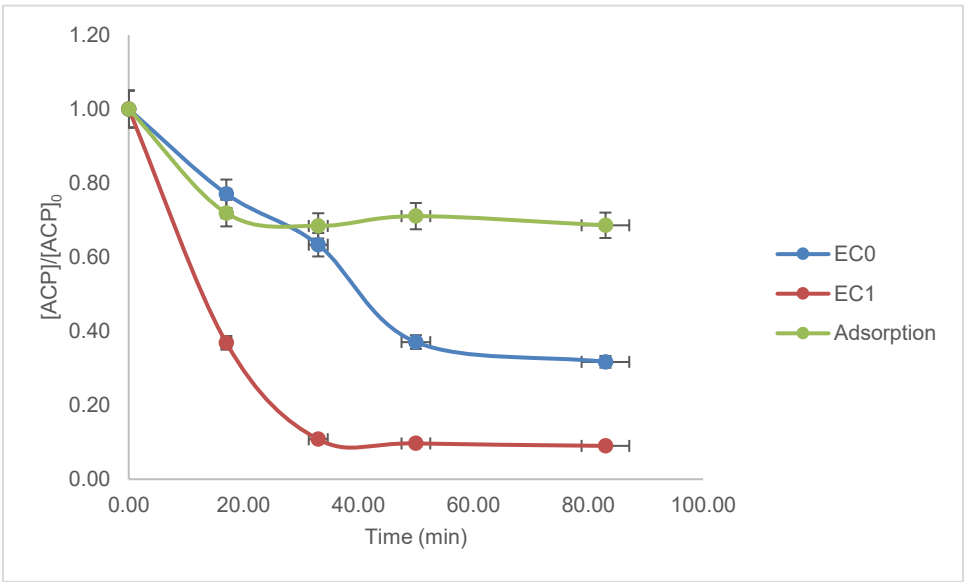


Figure 8 ACP degradation efficiency in systems with EC0, EC1 and adsorption as a function of time, with a concentration of [ACP] = 10 ppm, pH = 8, [EC0] = [EC1] = 1.5 g/L and irradiance of 924 $W/m^2$. (Source: made by the authors)

On the other hand, Figure 9 shows the Raman spectra corresponding to the amide I peak recorded during the in-situ monitoring of the photocatalytic reaction of ACP for the systems with EC0 and EC1. In these spectra, a progressive decrease in the area under the curve is observed as the reaction time progresses. Particularly, in the case of EC1, the

peak associated with amide I disappears completely after 33 minutes of reaction, evidencing its greater efficiency in the degradation of the compound.

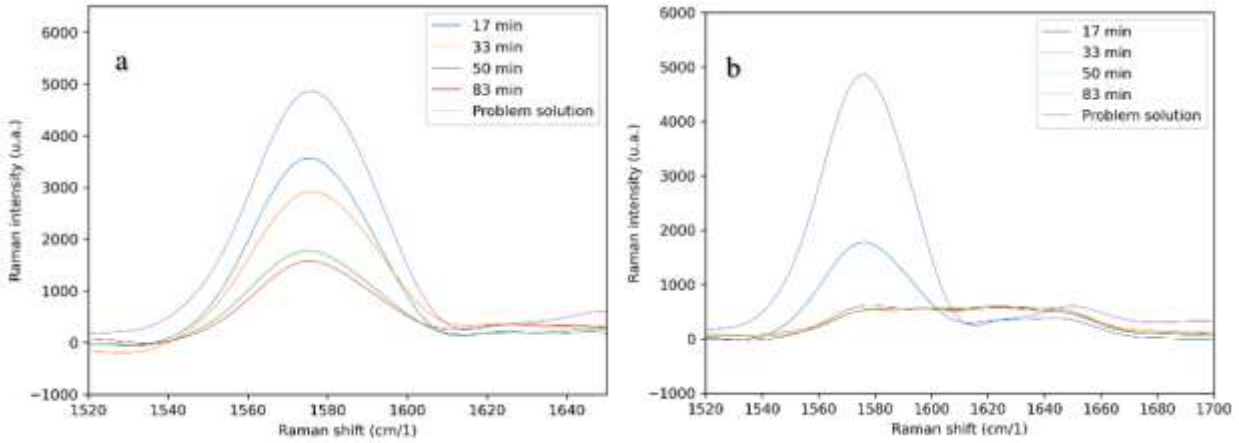


Figure 9 Photocatalytic degradation of ACP using ceramic foams with a loading of 1.5 g/L, monitored by Raman spectroscopy: EC0 (a) and EC1 (b). (Source: made by the authors)

The results obtained indicate that the combination of the $SiO_2$/Cu-$TiO_2$ NPs foam system, called EC1, presents a higher efficiency in the degradation of ACP compared to the control and EC0 experiments. This superiority in efficiency is attributed to the fact that, in the heterogeneous photocatalysis process, the catalyst is activated by high-energy photons. During these reactions, an electron from the valence band is promoted to the conduction band, generating a photohole in the semiconductor due to an external source of energy, in this case, natural solar radiation. The $TiO_2$ semiconductor, modified with $Cu^{2+}$ metal ions, plays a key role in preventing charge recombination, which optimizes the photocatalytic process. In addition, copper shifts the absorption spectrum towards lower energy regions, expanding the amount of usable radiation in the UV-visible range and contributing significantly to the overall performance of the process (Aguilar *et al*., 2022; Adamu *et al*., 2023).

## 4. Conclusions

Innovative photocatalytic ceramic foams have been developed using biogenic silica extracted from rice husks and $TiO_2$ NPs, both in their pure form and decorated with copper (EC0 and EC1, respectively). XRD characterization confirmed that $TiO_2$ is in its anatase phase, while analysis of the photocatalytic ceramic foams revealed the amorphous nature of the biogenic silica. On the other hand, the SEM-EDS study showed a rough morphology composed of a network of hemispherical particle agglomerates and confirmed the presence of copper in the EC1 ceramic foams.

The improvement in the photocatalytic activity of EC1 is attributed to a lower charge recombination rate and a longer lifetime of the photogenerated charges. This is because copper can induce doping states near the top of the valence band, which enhances the absorption in the visible spectrum through the Cu 3*d*-Ti 3*d* optical transition. In terms of performance, 91.0% degradation of ACP was achieved in a time of 83 min using a loading of 1.5 g/L of photocatalytic ceramic foam (EC1) under natural solar irradiation with an intensity of 924 W/m². This finding represents a significant advance in the photodegradation of emerging contaminants and provides valuable insights into the potential use of photocatalytic materials in the remediation of contaminated waters.

**Acknowledgements**

The abstract of this paper was presented at the Sustainable Water Management and Resource Adaptation: Security and Energy Nexus (SWMRA) Conference – 1st Edition, which was held on the 12th – 13th of November 2024.

The authors would like to express their gratitude to the National Fund for Science, Technology, and Innovation (Fonacit) for the funding provided to conduct this research, which is part of project No. 202300063. They also appreciate the valuable support provided by Dr. Paulino Betancourt, from the Center for Catalysis, Petroleum and Petrochemistry of the School of Chemistry of the Faculty of Sciences of the Central University of Venezuela.

**Funding declaration**

This research was funded by the National Fund for Science, Technology, and Innovation (Fonacit).

**Ethics approval**

Not applicable.

**Conflict of interest**

The authors declare that there is no competing interest.

**References**

Adamu, A., Isaacs, M., Boodhoo, K., & Abegão, F. R. (2023). Investigation of Cu/TiO2 synthesis methods and conditions for CO2 photocatalytic reduction via conversion of bicarbonate/carbonate to formate. *Journal of CO2 Utilization*, *70*(January), 102428. https://doi.org/10.1016/j.jcou.2023.102428

Aguilar, C., De la Cruz, A., Montalvo, C., Ruiz, A., Oros, S., Figueroa, S., Abatal, M., Anguebes, F., & Córdova, V. (2022). Effect of kinetics on the photocatalytic degradation of acetaminophen and the distribution of major intermediate with anatase-Ag synthesized by sol-gel under visible irradiation. *Frontiers in Environmental Science*, *10*(October), 1–11. https://doi.org/10.3389/fenvs.2022.943776

Borio, V., Vinha, R., Nicolau, R., De Oliveira, H., De Lima, C., & Silveira, L. (2012). Quantitative Evaluation of Acetaminophen in Oral Solutions by Dispersive Raman Spectroscopy for Quality Control. *Spectroscopy: An International Journal*, *27*(4), 215–228. https://doi.org/10.1155/2012/108041

Cailletaud, J., De Bleye, C., Dumont, E., Sacré, P. Y., Netchacovitch, L., Gut, Y., Boiret, M., Ginot, Y. M., Hubert, P., & Ziemons, E. (2018). Critical review of surface-enhanced Raman spectroscopy applications in the pharmaceutical field. *Journal of Pharmaceutical and Biomedical Analysis*, *147*, 458–472. https://doi.org/10.1016/j.jpba.2017.06.056

Cassano, A., & Alfano, O. (2000). Reaction engineering of suspended solid heterogeneous photocatalytic reactors. *Catalysis Today*, *58*(2–3), 167–197. https://doi.org/10.1016/S0920-5861(00)00251-0

Castillo, J., Arcuri, M., Vargas, V., & Piscitelli, V. (2022). Synthesis of nanocomposites SiO2@Co3O4, SiO2@ZnO, and SiO2@CuO from rice husks: spectroscopy and optical properties. *Applied Physics A*, *128*(2), 107. https://doi.org/10.1007/s00339-021-05247-5

De Bleye, C., Dumont, E., Rozet, E., Sacré, P. Y., Chavez, P. F., Netchacovitch, L., Piel, G., Hubert, P., & Ziemons, E. (2013). Determination of 4-aminophenol in a pharmaceutical formulation using surface enhanced Raman scattering: From development to method validation. *Talanta*, *116*, 899–905. https://doi.org/10.1016/j.talanta.2013.07.084

Dorraj, M., Alizadeh, M., Sairi, N., Basirun, W., Goh, B., Woi, P., & Alias, Y. (2017). Enhanced visible radiation photocatalytic activity of copper-doped titanium oxide–zinc oxide heterojunction for methyl orange degradation. *Applied Surface Science*, *414*, 251–261. https://doi.org/10.1016/j.apsusc.2017.04.045

Espiga, L. (2018). Materiales fotocatalíticos y sus aplicaciones en construcción [Universidad Politécnica de Catalunya]. In *Universidad Politecnica de Catalunya*. https://www.redalyc.org/pdf/115/11502906.pdf

Fernández, M., Matos, J., Montaña, R., Poon, P., Lanfredi, S., Praxedes, F., Hernández, J., Calvino, J., Rodríguez, E., Rodríguez, E., & Ania, C. (2019). Sunradiation photoactivity of rice husks-derived biogenic silica. *Catalysis Today*, *328*(December), 125–135. https://doi.org/10.1016/j.cattod.2018.12.008

Fujishima, A., & Honda, K. (1972). Electrochemical Photolysis of Water at a Semiconductor Electrode. *Nature*, *238*, 37–38.

Gonzalez, K., Quesada, I., Aleksandrova, F., Julcour, C., Andriantsiferana, C., Manero, M., Albasi, C., & Jáuregui, U. (2016). DEGRADATION OF PARACETAMOL IN AQUEOUS SOLUTION: COMPARISON OF DIFFERENT UV INDUCED ADVANCED OXIDATION PROCESSES. *Latin American Applied Research - An International Journal*, *46*(3), 115–120. https://doi.org/10.52292/j.laar.2016.341

Gupta, S., Gandhi, J., Kokate, S., Raikar, L., Gupta, V., & Prakash, H. (2023). Augmented photocatalytic degradation of Acetaminophen using hydrothermally treated g-C3N4 and persulfate under LED irradiation. *Heliyon*, *9*(5), e16450. https://doi.org/10.1016/j.heliyon.2023.e16450

Hoerudin, Setyawan, N., Suismono, Purwaningsih, H., & Apriliani, N. (2022). Morphology, Extraction Yield, and Properties of Biogenic Silica Nanoparticles from Indonesian Rice Husk as Influenced by Solvent Type and Aging Time. *IOP Conference Series: Earth and Environmental Science*, *1024*(1), 012076. https://doi.org/10.1088/1755-1315/1024/1/012076

Kaur, R., Kaur, A., Kaur, R., Singh, S., Bhatti, M., Umar, A., Baskoutas, S., & Kansal, S. (2021). Cu-BTC metal organic framework (MOF) derived Cu-doped TiO2 nanoparticles and their use as visible radiation active photocatalyst for the decomposition of ofloxacin (OFX) antibiotic and antibacterial activity. *Advanced Powder Technology*, *32*(5), 1350–1361. https://doi.org/10.1016/j.apt.2021.02.037

Leong, C. Y., Teh, H. L., Chen, M. C., & Lee, S. L. (2022). Effect of Synthesis Methods on Properties of Copper Oxide Doped Titanium Dioxide Photocatalyst in Dye Photodegradation of Rhodamine B. *Science and Technology Indonesia*, *7*(1), 91–97. https://doi.org/10.26554/sti.2022.7.1.91-97

Lin, J. C., Sopajaree, K., Jitjanesuwan, T., & Lu, M. (2018). Application of visible radiation on copper-doped titanium dioxide catalyzing degradation of chlorophenols. *Separation and Purification Technology*, *191*(June 2017), 233–243. https://doi.org/10.1016/j.seppur.2017.09.027

Manga, I., Rao, S., Lakshmi, D., Chandra, R., Padmaja, S., & Divya, G. (2019). Poly 3-Thenoic acid sensitized, Copper doped anatase/brookite TiO2 nanohybrids for enhanced photocatalytic degradation of an organophosphorus pesticide. *Journal of Environmental Chemical Engineering*, *7*(4), 103211. https://doi.org/10.1016/j.jece.2019.103211

Mojica, E., Zapata, J., Vedad, J., Desamero, R., & Dai, Z. (2018). Analysis of over-the-counter drugs using Raman spectroscopy. *ACS Symposium Series*, *1305*, 69–91. https://doi.org/10.1021/bk-2018-1305.ch005

Moongraksathum, B., Shang, J.-Y., & Chen, Y.-W. (2018). Photocatalytic Antibacterial Effectiveness of Cu-Doped TiO2 Thin Film Prepared via the Peroxo Sol-Gel Method. *Catalysts*, *8*(9), 352. https://doi.org/10.3390/catal8090352

Nevárez, M., Espinoza, P., Quiroz, F., & Ohtani, B. (2017). Fotocatálisis: inicio, actualidad y perspectivas a través del TiO2. *Avances En Química*, *12*, 45–59.

Ochuma, I., Osibo, O., Fishwick, R., Pollington, S., Wagland, A., Wood, J., & Winterbottom, M. (2007). Three-phase photocatalysis using suspended titania and titania supported on a reticulated foam monolith for water purification. *Catalysis Today*, *128*(1-2 SPEC. ISS.), 100–107. https://doi.org/10.1016/j.cattod.2007.05.015

Pereira, J., Castillo, J., & Labrador, H. (2023). Evaluación de las propiedades tribológicas y la viscosidad de un lubricante basado en un nanofluido de sílice ( $SiO_2$ ) Evaluation of the tribological properties and the viscosity of a lubricant based on a silica nanofluid ( $SiO_2$ ). *Revista Ciencia e Ingeniería*, *44*(December 2022), 79–88.

Porrang, S., Rahemi, N., Davaran, S., Mahdavi, M., & Hassanzadeh, B. (2021). Preparation and in-vitro evaluation of mesoporous biogenic silica nanoparticles obtained from rice and wheat husk as a biocompatible carrier for anti-cancer drug delivery. *European Journal of Pharmaceutical Sciences*, *163*(April), 105866. https://doi.org/10.1016/j.ejps.2021.105866

Preda, S., Pandele-Cușu, J., Petrescu, S., Ciobanu, E., Petcu, G., Culiță, D., Apostol, N., Costescu, R., Raut, I., Constantin, M., & Predoană, L. (2022). Photocatalytic and Antibacterial Properties of Doped TiO2 Nanopowders Synthesized by Sol−Gel Method. *Gels*, *8*(10), 673. https://doi.org/10.3390/gels8100673

Raheem, S., Sattar, J., & Al-Jubori, S. (2023). Characterization of Titanium dioxide (TiO2 ) Nanoparticles Biosynthesized using Leuconostoc spp. Isolated from Cow's Raw Milk. *Proceedings of the Pakistan Academy of Sciences: B. Life and Environmental Sciences*, *60*(1), 133–142. https://doi.org/10.53560/PPASB(60-1)823

Rodríguez, M., & Barrera, C. (2020). Procesos de oxidación avanzada en el tratamiento de agua. In *Publicaciones UAEM* (Primera ed, Vol. 1). Universidad Autónoma del Estado de México. http: //www.uaemex.mx

Shende, C., Smith, W., Brouillette, C., & Farquharson, S. (2014). Drug Stability Analysis by Raman Spectroscopy. *Pharmaceutics*, *6*(4), 651–662. https://doi.org/10.3390/pharmaceutics6040651

Shrestha, D., Nayaju, T., Kandel, M. R., Pradhananga, R., Park, C., & Kim, C. (2023). Rice husk-derived mesoporous biogenic silica nanoparticles for gravity chromatography. *Heliyon*, *9*(4), e15142. https://doi.org/10.1016/j.heliyon.2023.e15142

Srabovic, M., Huremovic, M., Catovic, B., & Muratovic, S. (2017). Design synthesis and crystallization of acetaminophen. *Journal of Chemical , Biological and Physical Sciences*, *7*(January), 218–230.

Turkten, N., Cinar, Z., Tomruk, A., & Bekbolet, M. (2019). Copper-doped TiO2 photocatalysts: application to drinking water by humic matter degradation. *Environmental Science and Pollution Research*, *26*(36), 36096–36106. https://doi.org/10.1007/s11356-019-04474-x

Ugarteburi, A. (2018). *Optimizacion de la reologia de componentes Fotocataliticos para aplicaciones avanzadas en elementos de fachada* [Universidad Politécnica de Catalunya]. http://upcommons.upc.edu/tesis

Warren, Z., Guaraldo, T., Martins, A., Wenk, J., & Mattia, D. (2023). Photocatalytic foams for water treatment: A systematic review and meta-analysis. *Journal of Environmental Chemical Engineering*, *11*(1), 109238. https://doi.org/10.1016/j.jece.2022.109238

Yang, L., Yu, L., & Ray, M. (2008). Degradation of paracetamol in aqueous solutions by TiO2 photocatalysis. *Water Research*, *42*(13), 3480–3488. https://doi.org/10.1016/j.watres.2008.04.023

Zhao, X., Wang, N., Zhu, M., Qiu, X., Sun, S., Liu, Y., Zhao, T., Yao, J., & Shan, G. (2022). Application of Transmission Raman Spectroscopy in Combination with Partial Least-Squares (PLS) for the Fast Quantification of Paracetamol. *Molecules*, *27*(5). https://doi.org/10.3390/molecules27051707